Square Voltage Power Supply Design Methodology for Dielectric Barrier Discharge Applications

Camilo Sanabria, Rafael Diez, Hubert Piquet, David Florez

Square voltage power supply design methodology for dielectric barrier discharge applications

Camilo Sanabria
Grupo de investigación en Robótica y Automatización-GIRA
Universidad Pedagógica y Tecnológica de Colombia
Sogamoso, Colombia
camilo.sanabria@uptc.edu.co

Rafael Diez
Electronics Enginnering Department
Pontificia Universidad Javeriana
Bogota, Colombia
rdiez@javeriana.edu.co

Hubert Piquet
LAPLACE Laboratory
Université de Toulouse, CNRS
Toulouse, France
piquet@laplace.univ-tlse.fr

David Florez
Electronics Engineering Department
Pontificia Universidad Javeriana
Bogota, Colombia
d.florez@javeriana.edu.co

***Abstract*— This paper presents a design methodology for a square pulse voltage source used in dielectric barrier discharge applications. This methodology considers electrical aspects of the discharge such as the average power to be delivered and the duration of the current pulses to properly size the switches and perform the magnetic design of the step-up transformer, where parameters such as leakage inductance and parasitic capacitance are considered for its design. The methodology was validated with the design and implementation of a voltage power supply for an experimental nitrogen oxides treatment bench.**

Keywords—Process design, Power supplies, Pulsed power systems, Dielectric barrier discharges.

I. Introduction

Dielectric barrier discharge (DBD) is a form of non-thermal plasma generation used in different applications, including ozone generation, ultraviolet radiation, air and water pollution treatment, and surface treatment [1]–[4]. DBD has advantages over other forms of non-thermal plasma generation, such as plasma stability and homogeneity of the discharge resulting from the presence of one or more dielectric layers [1].

Due to the presence of dielectric material between the DBD electrodes, the power sources used in these systems must supply a voltage on the order of a few kilovolts to several tens of kilovolts to achieve the discharge in the gas flowing through the dielectric material layers. This is a challenge for designers of power supplies for DBD applications.

Among the sources used to power DBD applications, pulse voltage sources are widely used because they are able to improve the processes associated with the use of non-thermal plasma over other types of sources [5], [6].

The square pulse voltage supply shown in Fig. 1 is one of the pulse sources used in different DBD applications. In [7], a set of equations explaining the behavior of the source when interacting with the DBD is presented for the first time. Prior to [7], the use of this source in experiments often required trial and error procedures to adjust parameters during experiments, such as the power delivered to the DBD [8]. Furthermore, one of the main problems of this topology for DBD applications was its design, so it was necessary to oversize the semiconductors and the transformer to ensure safe operation. Some of the most recent works study the development of compact supplies for DBDs however sacrificing output power rating [9], [10].

This paper proposes a design methodology for the so-called square voltage power source (SVPS) for DBD applications. We first outline the design steps for the source that makes up the methodology, and then we present its application in a DBD-based nitrogen oxide treatment system. Finally, the results of the source implementation are presented.

II. Power Supply Design Stages

A schematic of the SVPS feeding a DBD target of the design is shown in Fig. 1. This source comprises a full bridge-type voltage inverter, which is connected to the DBD via a step-up transformer. As demonstrated in [7], the transformer model considers the leakage inductance (L_k) of the transformer as an element interacting with the DBD, which determines the duration and intensity of the current pulses. An external inductance (L_{ext}) is added between the transformer and the bridge to adjust the desired duration of the current pulses in the DBD since the design aim is to have the smallest possible value of transformer leakage inductance.

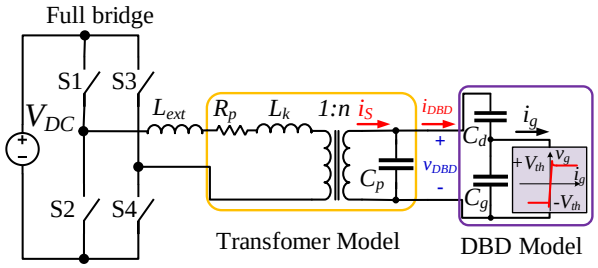

Fig. 1. Schematic circuit of the square voltage power supply (SVPS) fed to a DBD

The source schematic also includes a parasitic capacitance (C_p) and resistor (R_p), which gathers, the semiconductors and the transformer windings losses.

The behavior of the DBD can be modeled using an equivalent electrical circuit [11]–[13]. When the voltage in the DBD increases, the gas in the gap behaves as an insulator, and

the DBD is modeled as two series capacitances, an equivalent capacitance of the dielectric (C_d) and an equivalent capacitance of the gas (C_g). When the voltage in the gas reaches the threshold voltage (V_{th}), the gas behaves as a conductor, and discharge occurs. In this condition, the voltage in the gas remains almost constant and equal to V_{th}, and the model corresponds to the capacitance of the dielectric in series with a voltage source of V_{th} value. The values of the electrical model are determined using the Manley diagram (charge vs voltage diagram) of the DBD experimental data [14]–[16].

The proposed design methodology has been divided into four stages, as seen in the Fig. 2. The inputs for the design are the electric model of the DBD, the operating point, the assumptions, and the constraints. The operating point corresponds to the desired goals to be achieved by the source in the DBD, and they are electrical variables that affect the performance of the non-thermal plasma processes: DBD average power (P_{DBD}), duration of the first current pulse and switching frequency (f_s).

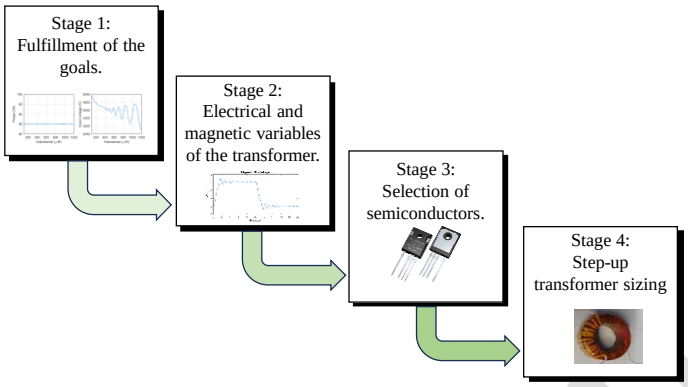

Fig. 2. Proposed stages for design of the SVPS for DBD applications.

The assumptions correspond to the values of the loss resistance (R_p), the parasitic capacitance (C_p), and the duration of the positive voltage pulse (t_p). The loss resistance affects the efficiency of the converter, and it should have a low value. The value of the parasitic capacitance connected in parallel to the DBD depends mainly on the transformer and the capacitance from the voltage probe used for the measurements. Because this capacitance is not easy to predict or adjust when building the transformer, and to simplify the design somewhat, its value is considered equal to zero. The effect of the capacitance on, for example, the DBD average power may be compensated in the implementation by the input voltage or the switching frequency.

Among the constraints we are aspects such as the maximum input voltage (V_{DC}), the number of transformer layers (proposed to be one for each winding in order to reduce the layer-to-layer parasitic capacitance [17]), the skin effect of the conductors, the insulation between windings and the availability of semiconductor elements and cores. As for the cores, it is proposed to use toroidal cores since it is possible to obtain more compact and lightweight transformers compared to conventional transformers [18], [19], and additionally, lower leakage inductance values are achieved [20].

A. *Stage 1: Fulfillment of the goals*

In this first stage, the values of input voltage and the leakage inductance that fulfill the design objectives are found. For this, the circuit in Fig. 1 is simplified by reflecting the elements on the primary side of the transformer to the secondary side. An optimization algorithm using the equations presented in [7] determines values of n^2L_k and nV_{DC} in the new equivalent circuit that meet the objectives.

One design assumption is the time the inverter switches must be switched to terminate the voltage pulse. This voltage pulse duration (t_p) is a function of the leakage inductance, so the optimization algorithm must adjust this value each time the value of n^2L_k changes. Equation (1) shows the expression used to calculate t_p, where C_{eq} is the equivalent capacitance of the DBD when no plasma is present.

$$t_p = \frac{3\pi}{\sqrt{\frac{1}{n^2 L_k C_{eq}} - \left(\frac{n^2 R_p}{2n^2 L_k}\right)^2}} \tag{1}$$

B. *Stage 2: Electrical and magnetic variables of the transformer.*

From the information of stage 1, in this stage, the maximum magnetic flux to be supported by the transformer is calculated, as well as the root mean square (*RMS*) values of the voltage and current of the DBD, which correspond to the voltage and current of the transformer secondary.

Regarding the calculation of the peak-to-peak magnetic flux linkage Ψ_{pp} (Wb) of the transformer as shown in [21], the following equation can be used on the positive voltage pulse of the DBD, where at the end of the pulse, the maximum value of magnetic flux occurs:

$$\Psi_{pp} = \int_0^{t_p} v_{DBD}(t)\,dt \tag{2}$$

C. *Stage 3: Selection of semiconductors*

At this stage, the design information and the maximum available input voltage constraint are used to determine the value of the turns ratio of the step-up transformer of the source and to select the semiconductors of the full bridge inverter.

For calculating the stress conditions of the semiconductors, it is essential to consider the transformer turns ratio since, if it is small, the semiconductor, for example, a MOSFET, must withstand a higher voltage between its drain-source terminals. In contrast, if the ratio is increased to have a lower DC voltage, the peak current that the MOSFET must withstand will increase.

D. *Stage 4: Step-up transformer sizing.*

Finally, in this stage, transformer sizing is performed to find the number of turns of the primary and secondary winding of the transformer. It should be noted that the leakage inductance of the transformer is minimized to obtain a value less than or equal to that determined in stage one of the SVPS design. If the value is less than that determined for the source, it is possible to add an inductor (L_{ext}) between the bridge and the transformer to achieve the desired value.

Although there are different types of cores for the magnetic design of the transformer, this work proposes using toroidal type cores due to the advantages of transformers built with them, such as a reduction in weight and volume and very low magnetic dispersion flux [18], [22]. Among the different manufacturers, a database with the technical characteristics of VACUUMSCHMELZE toroidal cores was elaborated, and Vitroperm 500F was selected as magnetic material [23].

The first step in this stage is to determine which cores can meet stage two's magnetic and electrical specifications using equation (3), which shows the relationship between core geometry and its power handling and voltage regulation capacity for the transformer [24].

$$\frac{W_a A_c^{\,2} K_u}{MLT} > \frac{P_t}{2K_e \alpha} \tag{3}$$

In equation (3), P_t corresponds to the apparent power, α is the regulation of the transformer, and the coefficient K_e relates to the magnetic and electric operating conditions. These values can be calculated as suggested in [24], where the value of the waveform coefficient K_f is defined in (6) as it exposed in [21], [24], [25]:

$$P_t = P_{DBD}\left(1+\frac{1}{\eta}\right)\sqrt{2} \tag{4}$$

$$K_e = 0.145 K_f^{\,2} f_s^{\,2} B_m^{\,2} \left(10^{-4}\right) \tag{5}$$

$$K_f = \frac{V_{DBDrms}}{\Psi_{pp} f_s} \tag{6}$$

Where η is the transformer efficiency, and B_m is the magnetic flux density from the core, which for the Vitroperm 500F cores can be selected between 0,4 to 0,8 T [22], [23], [26].

The other values of the equation (3) correspond to the iron area of the core A_c, the window utilization factor K_u, which is equal to 0.4 for toroidal cores [24], the window area W_a defined in (7), and the mean length turn *MLT* (8). I_D, O_D, and H are the inner diameter, outer diameter, and height of the core, respectively.

$$W_a = \left(\frac{I_D}{2}\right)^2 \pi \tag{7}$$

$$MLT = 0.8\left(O_D + 2H\right) \tag{8}$$

As a second step, the number of turns of the primary and secondary winding of the transformer is calculated for the cores that meet the condition of equation (3). The following equation calculates the number of turns of the primary winding:

$$N_p = \frac{V_{DBDrms}}{nK_f f_s B_m A_c}\left(10^4\right) \tag{9}$$

Finally, other transformer specification values are calculated at this stage, such as the copper and core losses and the transformer leakage inductance value. As mentioned above, one of the purposes of the transformer design is to have a small value of the leakage inductance, so estimating its value is essential to achieve the objectives of the source. The equation used for this estimation is presented below [22]:

$$L_k = \mu_o MLT_p \frac{N_p^{\,2}}{hw}\left[diso + \frac{dpri + d\,\mathrm{sec}}{3}\right] \tag{10}$$

Being μ_o the vacuum permeability, *MLTp* the mean length of the primary portion, *hw* the winding height, *diso* the isolation distance, *dpri* the thickness of the primary winding. and *dsec* the thickness of the secondary winding.

III. Sizing of an SVPS for a NO_X Treatment Application.

The results of using the previous SVPS design methodology are presented below for a DBD reactor of an experimental nitrogen oxide (NO_X) treatment bench. The input parameters for the design are:

- DBD average power $P_{DBD} = 85$ *W*.
- Duration of the first current pulse of *550 ns*.
- Switching frequency $f_s = 40$ *kHz*.
- DBD electrical model $C_d = 87$ *pF*, $C_g = 120$ *pF* and $Vth = 1750$ *V*.
- Loss resistance $n^2R_p = 300\ \Omega$
- Parasitic capacitance $C_p = 0$ *pF*.

The selection of the average power to be delivered to the reactor and the pulse duration of current is based on the experimental results obtained by Rueda in her doctoral thesis [27], who used a rectangular current source to test the NO_X reduction in the DBD reactor used in this design. The switching frequency was chosen considering that, with lower frequencies, the peak voltage that the transformer must withstand increases to reach the target power, and it is desired to maintain a voltage lower than *10 kV*. For frequencies higher than *40 kHz*, the maximum inductance value is limited to comply with the duration of the first current pulse due to the damping present in the source.

A. Stage 1

Fig. 3 shows the behavior of the power delivered by the source to the DBD and the corresponding value of nV_{DC} for a range of inductance values (n^2L_k) from *0.1 mH* to *1.2 mH*. These values and other electrical parameters of the design, such as the duration of the current pulses, are obtained using an optimization algorithm and the set of equations presented in [7] that explains the performance of the power supply when used to feed DBD systems. For this case, the following values were chosen: $nV_{DC} = 4656$ *V*, $n^2L_k = 430\ \mu H$, and $t_p = 1.39\ \mu s$.

B. Stage 2

Fig. 4 shows the circuit simulation results of Fig. 1, reflecting the elements on the primary side of the transformer to the secondary side and using the results of design stage 1. In Fig. 4a, the waveforms of the voltages at the load (DBD) and at the bridge are presented, while Fig. 4b. shows the waveforms of the current at the DBD and the gas current in the DBD model, where the presence of four discharges can be confirmed.

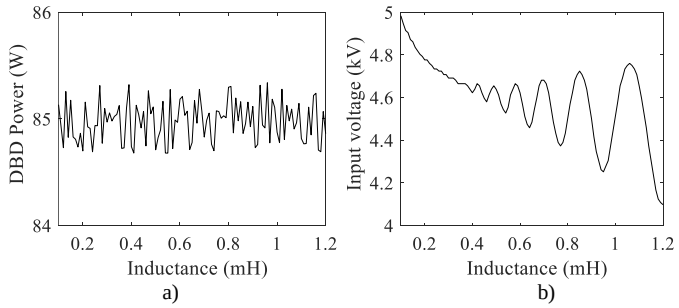

Fig. 3. Graphs of a) P_{DBD} vs n^2L_k; b) nV_{DC} vs n^2L_k;

The RMS (root mean square) values of the current and voltage in the secondary side of the transformer estimated from these simulation waveforms are *0.53A* and *2.11kV*, respectively. Likewise, the estimated magnetic flux linkage is *7.33 mWb*.

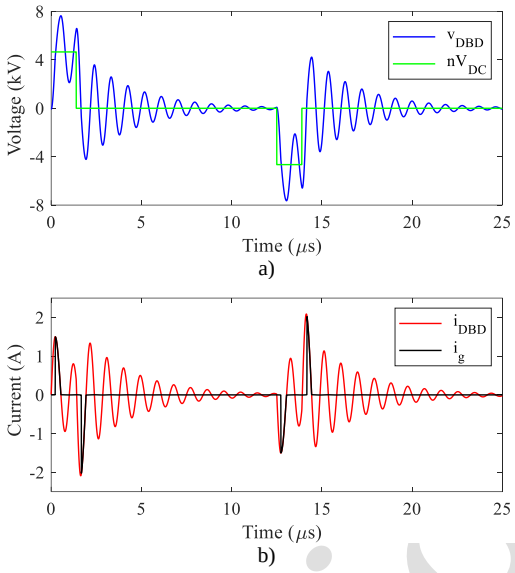

Fig. 4. Simulation results - stage 2. a) Circuit voltages; b) DBD currents

C. Stage 3

The maximum DC voltage available at the laboratory for the source is 600 V, a constraint that must be considered in selecting the step-up transformer turns ratio. For this case, a turns ratio equal to twelve (n=12) was selected, which leads to a VDC voltage of 388 V for the power supply. From simulation results, iDBD peak value is 2.2 A, therefore a maximum peak current in the transformer primary of 26.4 A is computed multiplying by the n ratio. With these values, we can determine the operating conditions of the semiconductor in the full-bridge voltage inverter since it must withstand the DC input voltage and the maximum peak current of the transformer primary at a switching frequency of 40 kHz. TABLE I presents the output values of this stage, including the estimated values of the transformer leakage inductance and the converter loss resistance, reflected in the primary side of the transformer (Fig. 1).

D. Stage 4

With the values obtained in the previous steps, we proceed to select a toroidal core for the step-up transformer of the source. In this step, a script developed in Matlab is used to compare different Vitroperm 500F toroidal cores of the T60006 series from the manufacturer VACUUMSCHMELZE [28]. The script determines the number of turns of the windings, core losses, and leakage inductance, among other data, delivering a list with the information for each one of the cores that meets the condition in (3). Of all possibilities, we are selecting the *L2080-V091* for the transformer. The number of turns for the primary and secondary are *6* and *72*, respectively. The theoretical leakage inductance (L_k) is *1.17 μH* (10), considering an insulation distance between the windings of *1 mm* for a breakdown voltage of *13.1 kV* (this insulation layer is made of Kapton tape) and distribution of the primary winding over the toroidal core of about *49°*.

TABLE I. STAGE 3 DESIGN RESULTS.

Parameter	Value
Turns ratio *n*	12
Leakage inductance L_k	2.99 μH
Loss resistance R_p	2.08 Ω
Input voltage V_{DC}	388 V
Peak current in the semiconductor	26.4 A

The Litz-type wire winding was chosen to calculate the winding resistances and the copper-related losses of the windings due to its advantages concerning a single wire and its availability in the laboratory. With the dimensions of the wires and the insulation between the windings of the transformer, we can sketch the mechanical dimensioning of the transformer, as shown in Fig. 5. Due to previous experiments with this type of core, we propose to wind the secondary first and then the primary, guaranteeing insulation between windings and between them and the core to reduce parasitic capacitances (C_p) and facilitate the winding of the transformer.

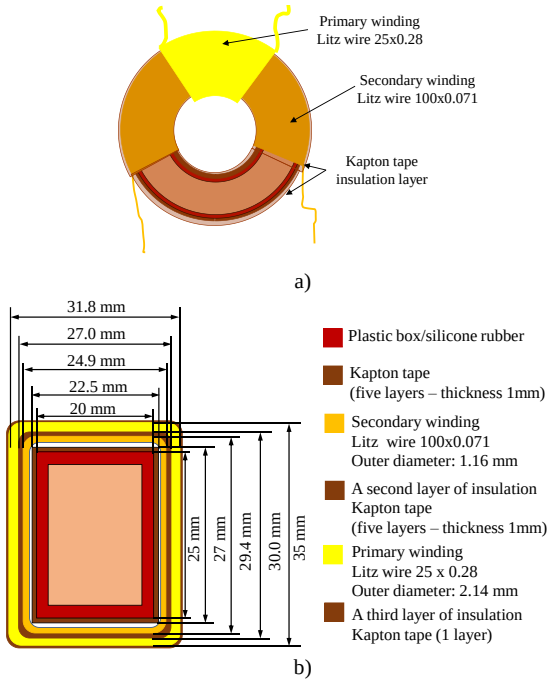

Fig. 5. Proposed Layout of the transformer. a) Top view, b) Side view.

Fig. 6 shows a schematic with the values determined in the design stages, the DBD specifications, and the assumptions made to design the power supply for the NO_X treatment system. It should be noted that adding an extra inductance of *1.82 μH*

between the inverter and the transformer was necessary to achieve the design leakage inductance value.

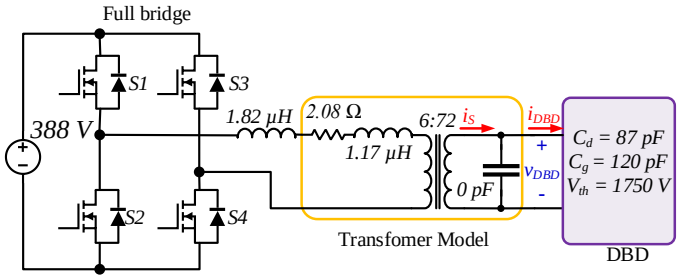

Fig. 6. Outcome of the SVPS design.

IV. Implementation of the SVPS

Fig. 7 shows a picture of the power supply source implemented for the NO_X treatment bench of the Laplace laboratory in Toulouse. The MOSFET selected is the GS66516B from GAN Systems company, with a drain-source voltage of *650 V*, a maximum drain pulse current of *120 A*, and a continuous current of *60 A*.

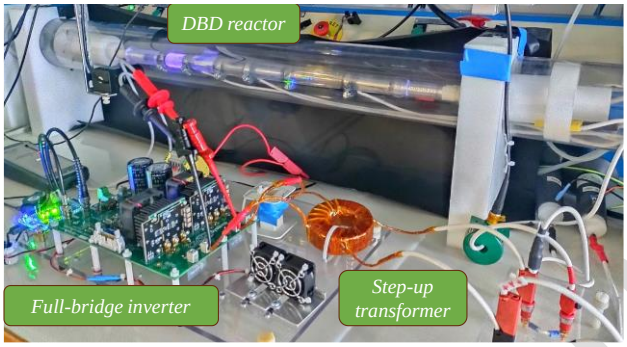

Fig. 7. SVPS implemented for a NOX treatment system through DBD.

The electrical characteristics of the transformer are determined using the model shown in Fig. 8 [29], performing a frequency analysis with the IM3570 Impedance Analyzer instrument. The tests performed correspond to the open circuit and short circuit tests from the transformer primary. Fig. 9 compares the frequency responses of the open circuit test (data in black color) and the theoretical results of the model (data in red color), showing a good match between the model and the transformer frequency data. The transformer parameters are: R_s = *60 mΩ*, L_k = *1.17 µH*, L_m = *0.34 mH*, R_p = *1.0 kΩ*, n = *12*, and C_p = *11.2 pF*.

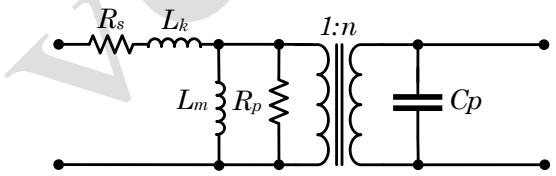

Fig. 8. Transformer model.

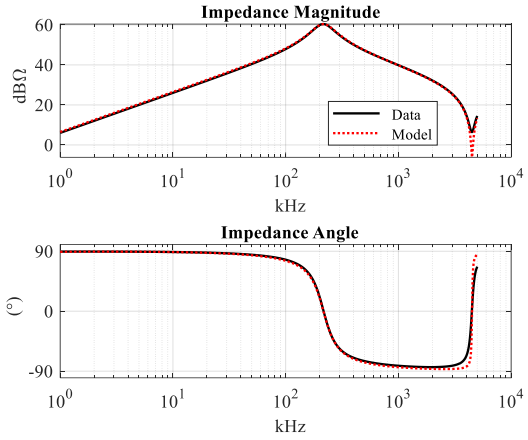

Fig. 9. Transformer frequency response, open circuit test.

The estimated loss resistance from the experimental power supply data was *3 Ω*. The value of the external inductance was adjusted to *0.85 µH* to obtain the design's voltage pulse duration because the values of the electrical model of the DBD and the C_p were different from those taken as specifications.

The SVPS implemented in the treatment bench can deliver power to the DBD from *30 W* up to 120 W. These powers were tested with input voltages from *400 V* to *480 V* and switching frequencies of *30 kHz* and *40 kHz*, withstanding a maximum peak voltage of *9.4 kV*. In Fig. 10, the experimental waveforms obtained for a VDC of 440 V and a fs of 40 kHz are shown.

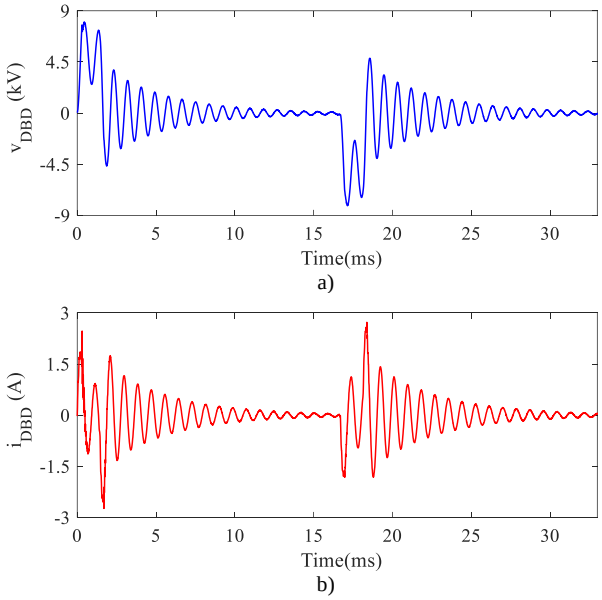

Fig. 10. Experimental waveforms: a) DBD voltage; b) DBD current.

V. Conclusions

This work proposes a sizing methodology for the square voltage source that allows the designer of power sources for DBD applications to consider electrical aspects of the DBD, such as the power delivered and the duration of the current pulses, as targets to be met in the design. To meet these objectives the methodology considers aspects such as the

electrical model parameters of the DBD reactor, the leakage inductance of the transformer, and constraints such as the available supply voltage, to determine the magnetic design of the transformer.

The experimental results show the methodology's usefulness, as the design specifications for a NOX treatment bench were met, and the exact value of leakage inductance estimated in the design stage was obtained for the transformer built.

VI. Acknowledgments

This work was financed in part by Departamento de Boyacá Scholarship Program. Convocatoria 779, Pontificia Universidad Javeriana Project No. ID SIAP 10035, Universidad Pedagógica y Tecnológica de Colombia, Laplace Laboratory.

References

[1] U. Kogelschatz, "Dielectric-barrier discharges: Their History, Discharge Physics, and Industrial Applications," *Plasma Chem. Plasma Process.*, vol. 23, no. 1, pp. 1–46, 2003, doi: 10.1023/A:1022470901385.

[2] C. Tendero, C. Tixier, P. Tristant, J. Desmaison, and P. Leprince, "Atmospheric pressure plasmas: A review," *Spectrochim. Acta Part B At. Spectrosc.*, vol. 61, no. 1, pp. 2–30, Jan. 2006, doi: 10.1016/j.sab.2005.10.003.

[3] H. E. Wagner, R. Brandenburg, K. V. Kozlov, A. Sonnenfeld, P. Michel, and J. F. Behnke, "The barrier discharge: Basic properties and applications to surface treatment," *Vacuum*, vol. 71, no. 3 SPEC., pp. 417–436, 2003, doi: 10.1016/S0042-207X(02)00765-0.

[4] P. J. Bruggeman, F. Iza, and R. Brandenburg, "Foundations of atmospheric pressure non-equilibrium plasmas," *Plasma Sources Sci. Technol.*, vol. 26, no. 12, p. 123002, Nov. 2017, doi: 10.1088/1361-6595/aa97af.

[5] X. Zhang, B. J. Lee, H. G. Im, and M. S. Cha, "Ozone Production with Dielectric Barrier Discharge: Effects of Power Source and Humidity," *IEEE Trans. Plasma Sci.*, vol. 44, no. 10, pp. 2288–2296, 2016, doi: 10.1109/TPS.2016.2601246.

[6] M. I. Lomaev, E. A. Sosnin, and V. F. Tarasenko, "Excilamps and their applications," *Prog. Quantum Electron.*, vol. 36, no. 1, pp. 51–97, 2012, doi: 10.1016/j.pquantelec.2012.03.003.

[7] C. Sanabria, D. Florez, H. Piquet, and R. Diez, "Sizing Equations for a Square Voltage Pulse Power Supply for Dielectric Barrier Discharges," *IEEE Trans. Power Electron.*, vol. 37, no. 4, pp. 4374–4384, 2022, doi: 10.1109/TPEL.2021.3122934.

[8] A. Zouaghi, A. Mekhaldi, R. Gouri, and N. Zouzou, "Analysis of nanosecond pulsed and square AC dielectric barrier discharges in planar configuration: Application to electrostatic precipitation," *IEEE Trans. Dielectr. Electr. Insul.*, vol. 24, no. 4, pp. 2314–2324, 2017, doi: 10.1109/TDEI.2017.006505.

[9] S. Jin *et al.*, "A High-Drive-Performance Microsecond Pulse Power Module for Portable DBD Plasma Source Device," *IEEE Trans. Power Electron.*, vol. 38, no. 12, pp. 15072–15085, 2023, doi: 10.1109/TPEL.2023.3315524.

[10] D. Florez, H. Piquet, E. Bru, and R. Diez, "Single-Switch Transformer-Less Power Supply for Low Temperature Plasma Jet - 3.3 kV SiC MOSFET Opportunities," *IEEE Trans. Power Electron.*, vol. 39, no. 6, pp. 7230–7237, 2024, doi: 10.1109/TPEL.2024.3372836.

[11] V. Rueda, A. Wiesner, R. Diez, and H. Piquet, "Enhancement of the DBD power for current-mode converters using the step-up transformer elements," in *2018 IEEE Industry Applications Society Annual Meeting, IAS 2018*, IEEE, Sep. 2018, pp. 1–8. doi: 10.1109/IAS.2018.8544496.

[12] X. Bonnin, J. Brandelero, N. Videau, H. Piquet, and T. Meynard, "A high voltage high frequency resonant inverter for supplying DBD devices with short discharge current pulses," *IEEE Trans. Power Electron.*, vol. 29, no. 8, pp. 4261–4269, 2014, doi: 10.1109/TPEL.2013.2295525.

[13] J. M. Alonso, M. Valdés, A. J. Calleja, J. Ribas, and J. Losada, "High Frequency Testing and Modeling of Silent Discharge Ozone Generators," *Ozone: Science and Engineering*, vol. 25, no. 5. pp. 363–376, 2003. doi: 10.1080/01919510390481685.

[14] A. V. Pipa, T. Hoder, J. Koskulics, M. Schmidt, and R. Brandenburg, "Experimental determination of dielectric barrier discharge capacitance," *Rev. Sci. Instrum.*, vol. 83, no. 7, 2012, doi: 10.1063/1.4737623.

[15] A. Laiadi, A. Chentouf, and Y. Laghmich, "Electrical modelling of homogeneous and filamentary dielectric barrier discharge at atmospheric pressure," *Mater. Today Proc.*, vol. 24, pp. 160–165, 2020, doi: 10.1016/j.matpr.2019.10.112.

[16] A. V. Pipa, J. Koskulics, R. Brandenburg, and T. Hoder, "The simplest equivalent circuit of a pulsed dielectric barrier discharge and the determination of the gas gap charge transfer," *Rev. Sci. Instrum.*, vol. 83, no. 11, 2012, doi: 10.1063/1.4767637.

[17] A. Baktash and A. Vahedi, "Calculation of parasitic elements in toroidal core transformers," *IEEE Trans. Plasma Sci.*, vol. 42, no. 6, pp. 1690–1696, 2014, doi: 10.1109/TPS.2014.2318757.

[18] M. Amirbande and A. Vahedi, "Calculation of Leakage Inductance in Toroidal Core Transformer with Non-Interleaved Windings," *IEEE Trans. Plasma Sci.*, vol. 48, no. 12, pp. 4215–4220, 2020, doi: 10.1109/TPS.2020.3035901.

[19] M. S. S. Nia, S. Saadatmand, M. Altimania, P. Shamsi, and M. Ferdowsi, "Analysis of Various Transformer Structures for High Frequency Isolation Applications," *51st North Am. Power Symp. NAPS 2019*, 2019, doi: 10.1109/NAPS46351.2019.9000392.

[20] H. Ataullah, T. Iqbal, I. U. Khalil, A. S. Mohammad, N. Ullah, and M. Emad Farrag, "Analysis and Verification of Leakage Inductance Calculation in DAB Converters Based on High-Frequency Toroidal Transformers under Different Design Scenarios," *Energies*, vol. 15, no. 17, 2022, doi: 10.3390/en15176176.

[21] A. Van den Bossche and V. C. Valchev, *Inductors and transformers for power electronics*. Taylor & Francis, 2005.

[22] D. Ruiz-Robles, V. Venegas-Rebollar, A. Anaya-Ruiz, E. L. Moreno-Goytia, and J. R. Rodríguez-Rodríguez, "Design and prototyping medium-frequency transformers featuring a nanocrystalline core for DC-DC converters," *Energies*, vol. 11, no. 8, 2018, doi: 10.3390/en11082081.

[23] D. Ruiz *et al.*, "Ferrites and Nanocrystalline Alloys Applied to DC–DC Converters for Renewable Energies," *Appl. Sci.*, vol. 12, no. 2, 2022, doi: 10.3390/app12020709.

[24] C. W. T. McLyman, *Transformer and Inductor Design Handbook*. CRC Press, 2017. doi: 10.1201/b10865.

[25] W. G. Hurley and W. H. Wölfle, *Transformers and inductors for power electronics: theory, design and applications*. Wiley-Blackwell, 2013.

[26] F. Allard, L. Pecastaing, M. Rivaletto, A. Ferron, J. P. Brasile, and S. Paquet, "Design and Electrical Simulations of a Resonant Transformer in a 200 Khz Dc-Dc Converter for Pulsed Power Applications," *Electrimacs, 2017, Toulouse, Fr. (hal-02154262)*, 2017.

[27] N. V. Rueda Algarra, "Reduction of Nitrogen Oxides in Diesel Exhaust using Dielectric Barrier Discharges driven by current-mode power supplies," Institut National Polytechnique de Toulouse, Pontificia Universidad Javeriana, 2022. [Online]. Available: https://oatao.univ-toulouse.fr/29661/

[28] Vaccuumschmelze, "EMC PRODUCTS based on NANOCRYSTALLINE VITROPERM," *PB-EMC EMC Prod. based NANOCRYSTALLINE Vitr. • Ed. 2016*, p. 28 pp., 2016, [Online]. Available: https://gmw.com/wp-content/uploads/2019/03/NanocrystallineVITROPERM-EMC-Products-2016_01.pdf

[29] D. M. Flórez Rubio, "Fuentes de alimentación eléctrica para el estudio y uso eficiente de lámparas excimer DBD," Pontificia Universidad Javeriana, 2020. doi: 10.11144/Javeriana.10554.16778.